

Ferroelectrically Controlled Chirality Switching of Weyl Quasiparticles

Zeling Li,^{1,2} Yu Liu,^{1,2} Le Du,^{1,2} Fengyu Li,^{1,2} Zhifeng Liu,^{1,3}
Lei Li,¹ Lei Wang,^{1,3,*} Botao Fu,^{4,†} and Xiao-Ping Li^{1,2,‡}

¹Research Center for Quantum Physics and Technologies,
School of Physical Science and Technology, Inner Mongolia University, Hohhot 010021, China

²Key Laboratory of Semiconductor Photovoltaic Technology and Energy
Materials at Universities of Inner Mongolia Autonomous Region,
Inner Mongolia University, Hohhot 010021, China

³Inner Mongolia Key Laboratory of Microscale Physics and Atom Innovation,
Inner Mongolia University, Hohhot 010021, China

⁴College of Physics and Electronic Engineering, Center for Computational Sciences,
Sichuan Normal University, Chengdu 610068, China

Weyl quasiparticles, as gapless low-energy excitations with nontrivial chirality, have garnered extensive interest in recent years. However, achieving effective and reversible control over their chirality (topological charge) remains a major challenge due to topological protection. In this work, we propose a ferroelectric mechanism to switch the chirality of Weyl phonons, where the reversal of ferroelectric polarization is intrinsically coupled to a simultaneous reversal of the chirality of Weyl points. This enables electric-field-driven control over the topological properties of phonon excitations. Through a comprehensive symmetry analysis of polar space groups, we identify 27 groups capable of hosting symmetry-protected Weyl phonons with chiral charges $C = 1, 2,$ and $3,$ whose chirality can be reversed via polarization switching. The first-principles calculations are performed to screen feasible material candidates for each type of chirality, yielding a set of prototypical ferroelectric compounds that realize the proposed mechanism. As a representative example, K_2ZnBr_4 hosts the minimal configuration of two pairs of Weyl phonons. Upon polarization reversal, the chirality of all Weyl points is inverted, accompanied by a reversal of associated topological features such as Berry curvature and surface phonon arcs. These findings provide a viable pathway for dynamic, electrical control of topological band crossings and open new avenues for chirality-based phononic applications.

Introduction. The past decade has witnessed the rapid development of topological semimetals and emergent quasiparticles, among which the most important type is Weyl quasiparticles [1–4]. In Weyl semimetals, the low-energy bands cross to form a singular twofold degenerate point in three dimensional (3D) momentum space, known as Weyl points. The existence of Weyl points requires the breaking of either time-reversal symmetry \mathcal{T} or inversion symmetry \mathcal{I} , so as to ensure their two-fold degeneracy. In addition, the existence of Weyl points does not require any other symmetry. Therefore, Weyl points can exist not only in electronic systems [5–13], but also in bosonic systems such as phonons [14–19]. A large number of materials hosting Weyl electrons [19–36] and Weyl phonons [37–53] have been predicted, and some of them have been experimentally verified [54–64].

As the most prominent topological feature, the Weyl point can be regarded as a point source of the Berry curvature field [1]. The Berry flux integral of Weyl point enclosed by a Gaussian sphere is a quantized topological charge, or chirality. The nontrivial chirality can give rise to fascinating phenomena, such as Fermi arc surface

states [4, 56–58], the chiral anomaly [65–70], chiral Landau levels [71–73] etc. This has motivated many efforts to modulate the chirality of Weyl points, reverse their sign, and thereby control the associated physical properties. For example, mechanical strain has been proposed to control the annihilation of Weyl points to change their chirality [74]. Other methods like magnetic field and optical approaches have also been reported to modulate chirality [75, 76]. Unfortunately, these methods all rely on external perturbations. An intrinsic mechanism and means of control are still highly desired.

Ferroelectricity, an intrinsic material property characterized by a switchable spontaneous polarization, is often coupled with diverse material functionalities and has been widely employed to modulate topological states. However, most of these studies have focused on ferroelectric control of topological insulators [77–83], while investigations into the ferroelectric modulation of Weyl semimetals remain scarce [84, 85]. This scarcity is primarily due to the strong Coulomb screening effect in metallic or semimetallic systems, which suppresses the formation of long-range ferroelectric order, thereby hindering the coexistence of ferroelectricity and topological semimetal phases in real materials. Crucially, this limitation applies mainly to electronic Weyl states. In contrast, the coupling between ferroelectricity and Weyl phonons is not constrained by electronic screening, thus opening

* lwang@imu.edu.cn

† fubotao2008@gmail.com

‡ xpli@imu.edu.cn

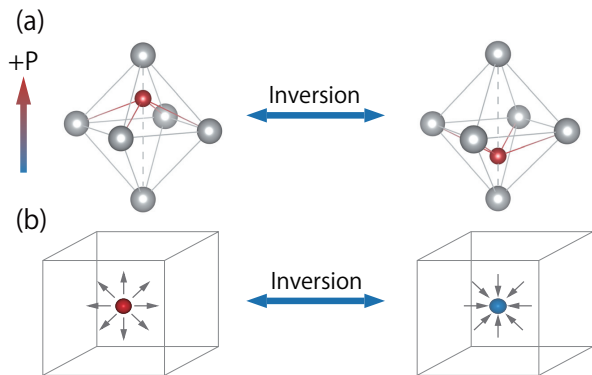


FIG. 1. Schematic of ferroelectric switchable chirality of Weyl points. (a) and (b) denote two ferroelectric structures connected by inversion symmetry, with opposite electric polarizations P . (c) and (d) represent the Weyl points in these structures, respectively, with opposite chiralities.

up a promising avenue for the realization and control of Weyl phonons via ferroelectric polarization.

In this Letter, we propose a general mechanism for controlling the chirality of Weyl phonons via ferroelectric switching. Using symmetry analysis, we show that both ferroelectric polarization and Weyl point chirality transform identically under improper symmetry operations. This symmetry correspondence enables polarization reversal to induce a chirality flip, offering a universal route for electrical control of topological phonon states. Guided by symmetry analysis, we systematically screen 27 polar space groups that can host symmetry-protected Weyl phonons with switchable chiralities of $C = \pm 1, \pm 2, \pm 3$. A set of prototypical ferroelectric materials exhibiting tunable phonon chirality is identified through high-throughput first-principles calculations. As a representative example, K_2ZnBr_4 hosts two pairs of Weyl phonons with chirality $C = \pm 1$ along a high-symmetry path. Upon polarization reversal, their chirality and associated topological features—including Berry curvature and surface states—undergo a complete sign change. Our work thus establishes a new principle for manipulating topological phonons and provides a realistic material platform for exploring electrically tunable chirality in crystalline solids.

Rationale and candidate space group. We analyze the principle of switching the chirality of Weyl points via ferroelectricity. Generally, two FE phases with opposite ferroelectric polarization strengths are connected by inversion symmetry \mathcal{I} (or mirror operation \mathcal{M}). Accordingly, it is natural to consider that the relevant physical quantities in these two FE phases would also be correlated through \mathcal{I} , which provides a foundation for tuning their properties. It should be noted that polar tensors and axial tensors of physical tensors exhibit distinct properties under symmetric transformations. For instance, as

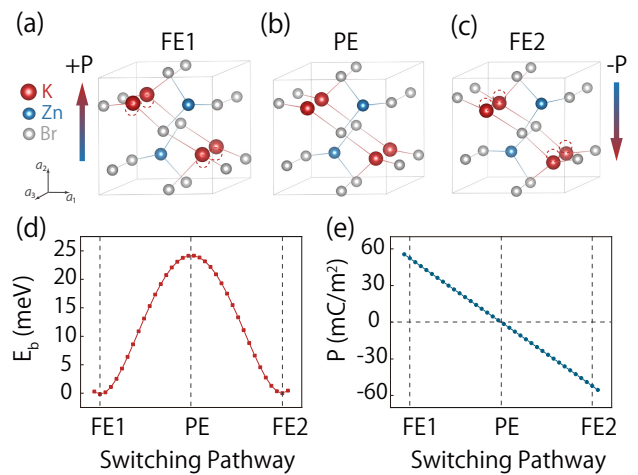


FIG. 2. (a) Structures of K_2ZnBr_4 in the FE1 state, (b) in the PE state, and (c) in the FE2 state. (d)-(e) show the calculated ferroelectric switching pathway and corresponding polarization in K_2ZnBr_4 .

a type of polar vector, the transformation of the electric polarization vector is given by $\mathbf{P} \xrightarrow{\mathcal{I}} -\mathbf{P}$ under \mathcal{I} [as shown in Fig. 1(a)]. In contrast, the Berry curvature, as an axial vector, transforms between the two ferroelectric phases under \mathcal{I} as $\Omega_1(\mathbf{k}) \xrightarrow{\mathcal{I}} \Omega_2(-\mathbf{k})$ (where 1 and 2 denote the two FE phases), with its sign unchanged. Since our target is the chirality switching of Weyl points, we need to focus on the transformation properties of the integral of the Berry curvature over a closed surface. Chirality can be expressed as $C = \frac{1}{2\pi} \oint_s \Omega(\mathbf{k}) \cdot d\mathbf{S}(\mathbf{k})$. Under the operation \mathcal{I} , although the direction of the Berry curvature does not change, the differential surface element vector undergoes a sign change, $d\mathbf{S}_1(\mathbf{k}) \xrightarrow{\mathcal{I}} -d\mathbf{S}_2(-\mathbf{k})$. As a result, the integral value C undergoes a sign reversal under \mathcal{I} [see Fig. 1(b)]. The chirality reversal can also be explained by a simple $k \cdot p$ model. In the FE phase, the Weyl point is described by $H_1 = \eta \mathbf{k} \cdot \boldsymbol{\sigma}$ with chirality $C = \text{sgn}(\eta)$. Under inversion \mathcal{I} , the polarization reverses, and the equation becomes $H_2 = -\eta \mathbf{k} \cdot \boldsymbol{\sigma}$, causing the chirality to flip to $C = \text{sgn}(-\eta)$. The scheme for controlling the chirality of Weyl points through ferroelectric polarization reversal has now been established.

We turn to investigate the candidate space groups for the ferroelectric control scheme. Fundamentally, the coexistence of the FE phase and the Weyl phase is crucial for achieving ferroelectric control. FE materials typically reside in specific polar space groups, all of which break inversion symmetry, thereby providing the possibility for the simultaneous existence of both the FE phase and the Weyl phase. Moreover, the existence of 3D Weyl points does not rely on additional symmetry protection. This implies that the effect of ferroelectric switching of phonon Weyl chirality can be realized in all polar space groups.

On the other hand, crystalline symmetries constrain

TABLE I. The candidate polar space groups that can host symmetry-protected Weyl points in spinless systems. SGs denotes the space group, and position denotes the high-symmetry point or high-symmetry line, where the Weyl points are located.

Type	SGs (position)	Species
HSL	3,4(Γ - Z , B - D , Y - C , A - E); 5(Γ - Z , A - M); 35-37(S - R); 44-46(T - W); 75-78(Γ - Z , M - A , X - R); 79-80(Γ - Z , Z - V , X - P); 143-145(Γ - A , K - H); 146(Γ - Z , Z - P); 156,158(K - H); 168-173(Γ - A , M - L , K - H); 75-78(Γ - Z , M - A); 79,80(Γ - Z , Z - V); 168-173(Γ - A); 168-173(Γ - A).	C-1 WP C-2 WP C-3 WP
HSP	80(P); 168,171,172(K , H); 169,170,173(K); 75,77(Γ , M , Z , A); 76,78(Γ , M); 79(Γ , Z , P); 80(Γ , Z); 143-145(Γ , A); 146(Γ , A); 168,171,172(Γ , A); 169,170,173(Γ).	C-1 WP C-2 WP

Weyl points to specific high-symmetry points and high-symmetry paths within the Brillouin zone, giving rise to symmetry-protected Weyl points. This constraint not only facilitates theoretical analysis but also greatly benefits high-throughput material screening and subsequent experimental exploration. Building on this idea, we systematically investigate the presence of symmetry-protected Weyl phonons in polar space groups and identify potential candidate groups. Specifically, for each polar space group, we examine the two-dimensional irreducible representations (IRRs) of the little groups associated with all high-symmetry points in the Brillouin zone, as well as the relevant one-dimensional IRRs along high-symmetry paths [86]. These IRRs serve as key indicators for the emergence of symmetry-protected Weyl points [12]. Based on the IRR characteristics, we construct corresponding $k \cdot p$ models and identify three types of Weyl points within the candidate groups: charge-1 (C-1), charge-2 (C-2), and charge-3 (C-3) Weyl points. The main results are summarized in Table I, with a more detailed version provided in the Supplemental Material (SM) [87], offering a guiding framework for identifying candidate materials.

High-quality material realization. Building on the symmetry-guided classification above, we further search for realizations of these Weyl phonons in experimentally synthesized ferroelectric materials with diverse crystal symmetries. Through high-throughput first-principles calculations, we identify high-quality candidate compounds for each type of Weyl phonon, and demonstrate their ferroelectrically switchable topological properties. Without loss of generality, we select K_2ZnBr_4 , which hosts C-1 Weyl phonons, as a representative example to demonstrate the electric-field-driven chirality switching of Weyl points in the main text, with other candidates of ferroelectric-switchable Weyl phonon materials with chirality $C = 1, 2$ and 3 presented in the SM [87].

K_2ZnBr_4 belongs to the ferroelectric family of A_2BX_4 -type compounds ($A = \text{Rb}, \text{K}$; $B = \text{Zn}, \text{Co}$; $X = \text{Cl}, \text{Br}, \text{I}$), which were successfully synthesized via aqueous solution methods and confirmed to exhibit ferroelectricity in 1990 [88]. Its ferroelectric phase adopts a monoclinic

structure with space group P2_1 (No. 4), which is among the candidate groups listed in Table I. We now focus on the reversible chirality switching behavior in K_2ZnBr_4 as a concrete demonstration of the proposed mechanism.

To examine the feasibility of polarization switching of K_2ZnBr_4 , we calculated the FE switching pathway and identified a centrosymmetric paraelectric (PE) phase [see Fig. 2]. The crystal structure of PE phase is shown in Fig. 2(b), where the K atoms are surrounded by ZnBr_4 units and possess the symmetry of space group $\text{P2}_1/\text{m}$ (No. 11). Upon displacement of the K atoms along the b -axis, the system presents two energetically degenerate FE ground states (FE1 and FE2) with opposite polarizations [see Fig. 2(a) and (c)]. Moreover, the two FE states are related by the inversion operation \mathcal{I} . Once Weyl points emerge in the phonon spectra of the FE phase, the effect of switching the chirality of Weyl points through ferroelectric switching can be realized.

We then calculate the phonon band structure of the FE1 state along high-symmetry paths in Brillouin zone (BZ). The FE1 state of K_2ZnBr_4 belongs to the SG 4, which, according to Table I, may host Weyl points on the E - A , Y - C , B - D or Γ - Z paths owing to accidental band crossings. Here, we plot the phonon bands within the frequency range of 1.6 to 2.1 THz, as illustrated in Fig. 3(a) (the whole spectrum can be found in SM [87]). One observes that there are indeed two WPs located on the E - A and Y - C paths, formed by the crossing of two phonon branches No. 14 and No. 15, which are protected by a twofold screw-rotation $\widetilde{C}_{2y} = \{C_{2y}|0\frac{1}{2}0\}$. In addition, time-reversal symmetry results in the existence of two additional Weyl points on the opposite paths. A careful scan reveals that apart from these four WPs, the 14th and 15th bands do not form any other band degeneracies. Thus, the system contains only two pairs of Weyl points, which is the minimal number allowed in nonmagnetic materials.

The four Weyl points are labeled as $W_{i=1,2,3,4}$, and their distribution in the BZ is shown in Fig. 3(b), where the red and blue balls represent chiralities of +1 and -1, respectively [87]. Moreover, the $k \cdot p$ effective Hamiltonian of the four Weyl points $W_{i=1,2,3,4}$ share an identical form,

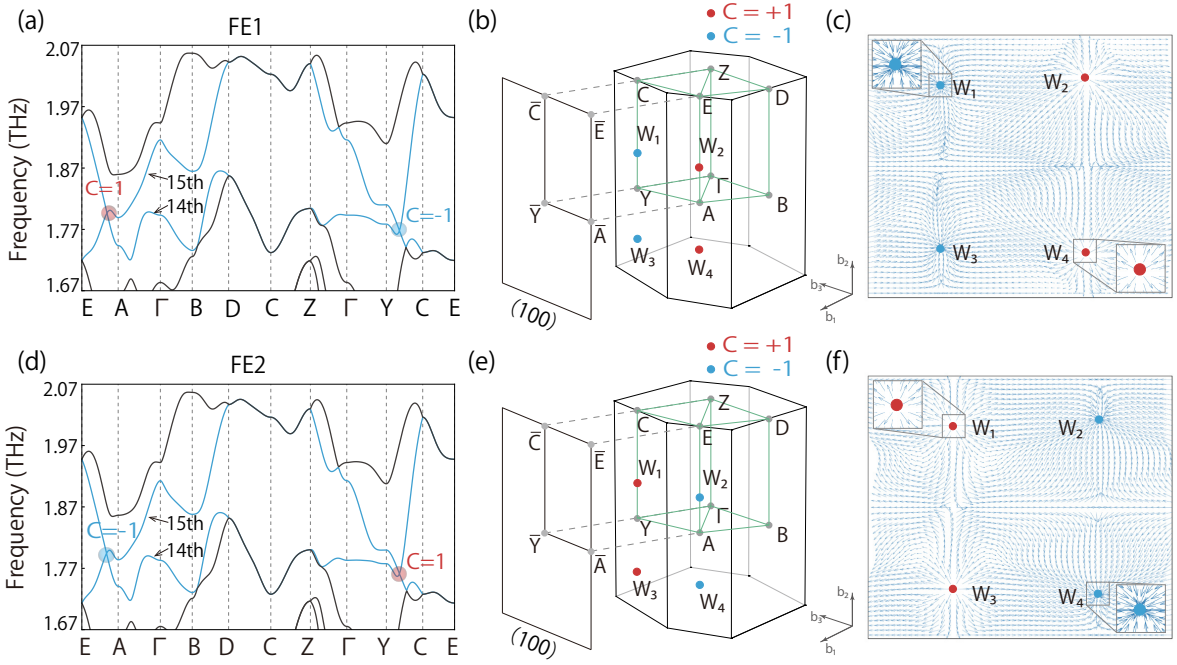


FIG. 3. (a), (b), and (c) respectively show the calculated phonon spectrum, the bulk and surface BZs, and the distribution of Berry curvature in the $k_x = \pi$ for K_2ZnBr_4 in FE1 state. Similarly, (d)-(f) correspond to the same properties of K_2ZnBr_4 in the FE2 state. The phonon branches forming the Weyl points are highlighted by blue curves.

given by [87]

$$\mathcal{H}(\mathbf{k}) = \sigma_0(c_1 + c_2 k_z) + c_3 \sigma_3 k_z + \sum_{j=1}^2 \sigma_j (c_{j,1} k_x + c_{j,2} k_y), \quad (1)$$

with σ_i ($i = 1, 2, 3$) the Pauli matrix and σ_0 the identity matrix, here $c_{i=1,2,3}$, $c_{j,1}$ and $c_{j,2}$ ($j = 1, 2$) are real parameters. According to Eq. (1), the band splitting around the WPs is linear, implying that these Weyl points have chirality of ± 1 , which agrees with our calculations.

Furthermore, we turn to investigating the change of chirality of Weyl points in K_2ZnBr_4 under ferroelectric switching. The phonon spectrum of the FE2 state is presented in Fig. 3(d). It is important to note that the two polarization states give identical dispersions, as it should be. Naturally, the distribution of Weyl points in the two polarization states is also completely identical, but the chirality of the Weyl points is different. The calculated chirality of the Weyl points in the FE2 state is shown in Fig. 3(e), where one can observe that their value has flipped signs compared to those in FE1, indicating the realization of the sign reversal of Weyl phonon chirality under ferroelectric switching.

Switching of topological properties. In addition to chirality, other topological quantities associated with Weyl points may also exhibit a flip during the ferroelectric switching. Among them, the Berry curvature field, as a significant quantity that characterizes the singularity

of Weyl points with a “source” or a “sink”, exhibits a divergent geometric feature in the vicinity of the Weyl points [1]. Thus, it will inevitably undergo redistribution with the change of Weyl point chirality. We then plot the Berry curvature fields for two FE states on the E - C - Y - A plane in the BZ. The results are shown in Fig. 3(c) and (f), respectively.

One can see that the two polarization phases exhibit completely opposite distribution characteristics. Specifically, near the Weyl point W_1 , the Berry curvature in the FE1 state emanates from the Weyl point [see Fig. 3(c)], while in the FE2 state, it is absorbed and converges at the same Weyl point [see Fig. 3(f)]. The Berry curvatures of the other three Weyl points also exhibit similar opposite distributions in the two FE states and are consistent with their respective chiralities.

Another important quantity associated with the chirality of Weyl points is the topological surface state. It has been recognized that surface states of Weyl points exhibit a helicoid band structure surrounding the surface projections of the points, which can be described by a non-compact Riemann surface [89]. Notably, the helicoid direction of surface states is determined by the chirality of the Weyl point, and thus it may be reversed by changing chirality. To verify this idea, we calculated the surface states of the (100) surface for K_2ZnBr_4 in two FE states [see Fig. 4]. In Fig. 4(a)-(b), the surface BZ with projected Weyl points is presented, while Fig. 4(c)-(d) show the corresponding Fermi arc states.

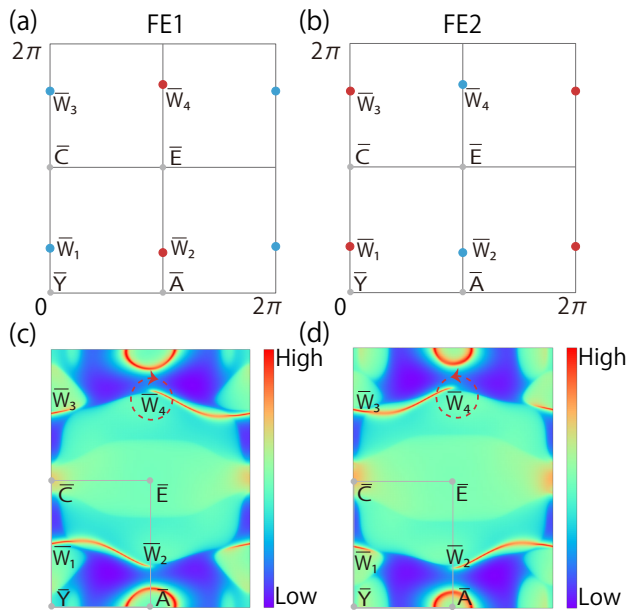


FIG. 4. (a) and (b) show the (100) surface BZ of K_2ZnBr_4 for FE1 and FE2 states, with $\bar{W}_{i=1,2,3,4}$ indicating projected Weyl points. (c) and (d) show the projected spectra on the (001) surface for FE1 and FE2 states. The red dashed circles indicate the helical direction of surface states near Weyl points.

One can observe that in both FE1 and FE2 states, a Fermi arc connects the projection of each Weyl point to another with opposite chirality, indicating a ± 1 chirality of bulk Weyl points. However, the surface states show opposite helicoid structures in FE1 and FE2. For instance, considering the projected Weyl point \bar{W}_4 , if the surface state around \bar{W}_4 in FE1 is defined as helicoid [see Fig. 4(c)], it appears as antihelicoid in FE2 [see Fig. 4(d)]. This switching with opposite helicoid is also applicable to other projected Weyl points, enabling the ferroelectric switching of the helicoid direction of topological surface states.

It is particularly noteworthy that the topological charge of Weyl phonons plays a crucial role when they interact with other quasiparticles, such as electrons and photons. This makes the electric control of phonon chirality not only a fundamental advance in topological phononics, but also a powerful tool for manipulating diverse physical processes in ferroelectric systems [90, 91]. As illustrated in Figs. 5(a)–(b), we designed a device for the electrically controlled nonlinear phonon Hall effect (NPHE) based on K_2ZnBr_4 material [87]. Applying a transverse temperature gradient ($\Delta_x \mathbf{T}$) to K_2ZnBr_4 induces a longitudinal nonlinear thermal current (\mathbf{j}_y), whose direction is directly linked to the Berry curvature of the Weyl phonons. Remarkably, reversing the ferroelectric polarization via an external electric field flips the phonon chirality and thus reverses the nonlinear thermal

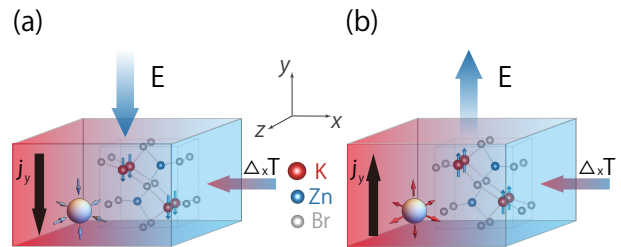


FIG. 5. Schematic diagram of the NPHE under the temperature gradient, where E represents the applied external electric field. The black arrows indicate the deflection of the nonlinear thermal current.

current \mathbf{j}_y . This electrically-driven reversal provides a clear and experimentally accessible signature of chirality switching, highlighting the potential of ferroelectric Weyl systems for functional topological control and phonon-based information processing.

Conclusion. In summary, we present a general symmetry-based framework for electrically controlling the topological properties of Weyl phonons—including chirality, Berry curvature, and helicoid surface states—through displacement-type ferroelectricity. By systematically analyzing polar space groups, we identify 27 candidate symmetries that can host symmetry-protected Weyl phonons with tunable topological charges, providing a concrete guideline for the targeted search of real material realizations. Our high-throughput first-principles screening further reveals that experimentally synthesized ferroelectrics, such as K_2ZnBr_4 and its structural family, as well as $Y(OH)_3$ and $LiIO_3$ [87], are ideal platforms for realizing electric-field-driven Weyl chirality switching in phononic systems. In contrast to conventional tuning methods (e.g., magnetic fields, strain, or doping), our approach utilizes the intrinsic, reversible polarization of ferroelectrics for robust and scalable topological control. This offers a promising strategy for developing phononic and information devices, with potential applications in phononic logic, spin-heat conversion, and nonreciprocal thermal transport.

This work is supported by the National Natural Science Foundation of China (Grant No. 12304086, Grant No. 12304165, Grant No. 12204330).

-
- [1] N. P. Armitage, E. J. Mele, and A. Vishwanath, Weyl and Dirac semimetals in three-dimensional solids, *Rev. Mod. Phys.* **90**, 015001 (2018).
 - [2] C. Herring, Accidental degeneracy in the energy bands of crystals, *Phys. Rev.* **52**, 365 (1937).
 - [3] S. Murakami, Phase transition between the quantum spin Hall and insulator phases in 3D: emergence of a topolog-

- ical gapless phase, *New J. Phys.* **9**, 356 (2007).
- [4] X. Wan, A. M. Turner, A. Vishwanath, and S. Y. Savrasov, Topological semimetal and Fermi-arc surface states in the electronic structure of pyrochlore iridates, *Phys. Rev. B* **83**, 205101 (2011).
- [5] G. Xu, H. Weng, Z. Wang, X. Dai, and Z. Fang, Chern Semimetal and the Quantized Anomalous Hall Effect in HgCr_2Se_4 , *Phys. Rev. Lett.* **107**, 186806 (2011).
- [6] A. A. Burkov and L. Balents, Weyl Semimetal in a Topological Insulator Multilayer, *Phys. Rev. Lett.* **107**, 127205 (2011).
- [7] A. A. Burkov, M. D. Hook, and L. Balents, Topological nodal semimetals, *Phys. Rev. B* **84**, 235126 (2011).
- [8] C. Fang, M. J. Gilbert, X. Dai, and B. A. Bernevig, Multi-Weyl Topological Semimetals Stabilized by Point Group Symmetry, *Phys. Rev. Lett.* **108**, 266802 (2012).
- [9] G. B. Halász and L. Balents, Time-reversal invariant realization of the Weyl semimetal phase, *Phys. Rev. B* **85**, 035103 (2012).
- [10] J. Liu and D. Vanderbilt, Weyl semimetals from noncentrosymmetric topological insulators, *Phys. Rev. B* **90**, 155316 (2014).
- [11] H. Weng, C. Fang, Z. Fang, B. A. Bernevig, and X. Dai, Weyl Semimetal Phase in Noncentrosymmetric Transition-Metal Monophosphides, *Phys. Rev. X* **5**, 011029 (2015).
- [12] Z.-M. Yu, Z. Zhang, G.-B. Liu, W. Wu, X.-P. Li, R.-W. Zhang, S. A. Yang, and Y. Yao, Encyclopedia of emergent particles in three-dimensional crystals, *Sci. Bull.* **67**, 375 (2022).
- [13] A. A. Soluyanov, D. Gresch, Z. Wang, Q. Wu, M. Troyer, X. Dai, and B. A. Bernevig, Type-II weyl semimetals, *Nature* **527**, 495 (2015).
- [14] Y. Liu, Y. Xu, S.-C. Zhang, and W. Duan, Model for topological phononics and phonon diode, *Phys. Rev. B* **96**, 064106 (2017).
- [15] W.-C. Ji and J.-R. Shi, Topological phonon modes in a two-dimensional Wigner crystal, *Chin. Phys. Lett.* **34**, 036301 (2017).
- [16] T. Zhang, Z. Song, A. Alexandradinata, H. Weng, C. Fang, L. Lu, and Z. Fang, Double-Weyl Phonons in Transition-Metal Monosilicides, *Phys. Rev. Lett.* **120**, 016401 (2018).
- [17] J. Li, Q. Xie, S. Ullah, R. Li, H. Ma, D. Li, Y. Li, and X.-Q. Chen, Coexistent three-component and two-component Weyl phonons in TiS , ZrSe , and HfTe , *Phys. Rev. B* **97**, 054305 (2018).
- [18] B. W. Xia, R. Wang, Z. J. Chen, Y. J. Zhao, and H. Xu, Symmetry-Protected Ideal Type-II Weyl Phonons in CdTe , *Phys. Rev. Lett.* **123**, 065501 (2019).
- [19] J. Liu, W. Hou, E. Wang, S. Zhang, J.-T. Sun, and S. Meng, Ideal type-II Weyl phonons in wurtzite CuI , *Phys. Rev. B* **100**, 081204 (2019).
- [20] F. Tang, H. C. Po, A. Vishwanath, and X. Wan, Comprehensive search for topological materials using symmetry indicators, *Nature* **566**, 486 (2019).
- [21] M. Vergniory, L. Elcoro, C. Felser, N. Regnault, B. A. Bernevig, and Z. Wang, A complete catalogue of high-quality topological materials, *Nature* **566**, 480 (2019).
- [22] S.-M. Huang, S.-Y. Xu, I. Belopolski, C.-C. Lee, G. Chang, B. Wang, N. Alidoust, G. Bian, M. Neupane, C. Zhang, *et al.*, A Weyl Fermion semimetal with surface Fermi arcs in the transition metal monpnictide TaAs class, *Nat. Commun.* **6**, 7373 (2015).
- [23] Y. Sun, S.-C. Wu, M. N. Ali, C. Felser, and B. Yan, Prediction of Weyl semimetal in orthorhombic MoTe_2 , *Phys. Rev. B* **92**, 161107 (2015).
- [24] J. Ruan, S.-K. Jian, D. Zhang, H. Yao, H. Zhang, S.-C. Zhang, and D. Xing, Ideal Weyl Semimetals in the Chalcopyrites CuTiSe_2 , AgTiTe_2 , AuTiTe_2 , and ZnPbAs_2 , *Phys. Rev. Lett.* **116**, 226801 (2016).
- [25] G. Autès, D. Gresch, M. Troyer, A. A. Soluyanov, and O. V. Yazyev, Robust Type-II Weyl Semimetal Phase in Transition Metal Diphosphides XP_2 ($X = \text{Mo}, \text{W}$), *Phys. Rev. Lett.* **117**, 066402 (2016).
- [26] Z. Wang, M. G. Vergniory, S. Kushwaha, M. Hirschberger, E. V. Chulkov, A. Ernst, N. P. Ong, R. J. Cava, and B. A. Bernevig, Time-Reversal-Breaking Weyl Fermions in Magnetic Heusler Alloys, *Phys. Rev. Lett.* **117**, 236401 (2016).
- [27] W. Shi, L. Muechler, K. Manna, Y. Zhang, K. Koepnik, R. Car, J. van den Brink, C. Felser, and Y. Sun, Prediction of a magnetic Weyl semimetal without spin-orbit coupling and strong anomalous Hall effect in the Heusler compensated ferrimagnet Ti_2MnAl , *Phys. Rev. B* **97**, 060406 (2018).
- [28] Q. Xu, E. Liu, W. Shi, L. Muechler, J. Gayles, C. Felser, and Y. Sun, Topological surface Fermi arcs in the magnetic Weyl semimetal $\text{Co}_3\text{Sn}_2\text{S}_2$, *Phys. Rev. B* **97**, 235416 (2018).
- [29] S.-Y. Xu, N. Alidoust, G. Chang, H. Lu, B. Singh, I. Belopolski, D. S. Sanchez, X. Zhang, G. Bian, H. Zheng, *et al.*, Discovery of Lorentz-violating type II Weyl fermions in LaAlGe , *Sci. Adv.* **3**, e1603266 (2017).
- [30] K. Koepnik, D. Kasinathan, D. V. Efremov, S. Khim, S. Borisenko, B. Büchner, and J. van den Brink, TaIrTe_4 : A ternary type-II Weyl semimetal, *Phys. Rev. B* **93**, 201101 (2016).
- [31] G. Chang, B. J. Wieder, F. Schindler, D. S. Sanchez, I. Belopolski, S.-M. Huang, B. Singh, D. Wu, T.-R. Chang, T. Neupert, *et al.*, Topological quantum properties of chiral crystals, *Nat. Mater.* **17**, 978 (2018).
- [32] L.-L. Wang, N. H. Jo, B. Kuthanazhi, Y. Wu, R. J. McQueeney, A. Kaminski, and P. C. Canfield, Single pair of Weyl fermions in the half-metallic semimetal EuCd_2As_2 , *Phys. Rev. B* **99**, 245147 (2019).
- [33] S.-M. Huang, S.-Y. Xu, I. Belopolski, C.-C. Lee, G. Chang, T.-R. Chang, B. Wang, N. Alidoust, G. Bian, M. Neupane, *et al.*, New type of Weyl semimetal with quadratic double Weyl fermions, *Proc. Natl. Acad. Sci.* **113**, 1180 (2016).
- [34] X.-P. Li, K. Deng, B. Fu, Y. Li, D.-S. Ma, J. Han, J. Zhou, S. Zhou, and Y. Yao, Type-III Weyl semimetals: $(\text{TaSe}_4)_2\text{I}$, *Phys. Rev. B* **103**, L081402 (2021).
- [35] G. Chang, S.-Y. Xu, H. Zheng, B. Singh, C.-H. Hsu, G. Bian, N. Alidoust, I. Belopolski, D. S. Sanchez, S. Zhang, *et al.*, Room-temperature magnetic topological Weyl fermion and nodal line semimetal states in half-metallic Heusler Co_2TiX ($X = \text{Si}, \text{Ge}, \text{or Sn}$), *Sci. Rep.* **6**, 38839 (2016).
- [36] B. Yan and C. Felser, Topological materials: Weyl semimetals, *Annu. Rev. Condens. Matter Phys.* **8**, 337 (2017).
- [37] Y. Xu, M. Vergniory, D.-S. Ma, J. L. Mañes, Z.-D. Song, B. A. Bernevig, N. Regnault, and L. Elcoro, Catalog of topological phonon materials, *Science* **384**, eadf8458 (2024).
- [38] Q.-B. Liu, Y. Qian, H.-H. Fu, and Z. Wang, Symmetry-

- enforced Weyl phonons, *npj Comput. Mater.* **6**, 95 (2020).
- [39] J. Li, J. Liu, S. A. Baronett, M. Liu, L. Wang, R. Li, Y. Chen, D. Li, Q. Zhu, and X.-Q. Chen, Computation and data driven discovery of topological phononic materials, *Nat. Commun.* **12**, 1204 (2021).
- [40] T. Yang, J. Wang, X.-P. Li, X. Wang, Z. Cheng, W. Wang, and G. Zhang, Topological nodal-point phononic systems, *Matter* **7**, 320 (2024).
- [41] P. Qin, G. Liu, P. Wu, and H. Xu, Diverse degeneracy types in topological phonons: A perspective, *Appl. Phys. Lett.* **124** (2024).
- [42] Z.-K. Ding, Y.-J. Zeng, W. Liu, L.-M. Tang, and K.-Q. Chen, Topological phonons and thermoelectric conversion in crystalline materials, *Adv. Funct. Mater.* **34**, 2401684 (2024).
- [43] R. Wang, B. W. Xia, Z. J. Chen, B. B. Zheng, Y. J. Zhao, and H. Xu, Symmetry-Protected Topological Triangular Weyl Complex, *Phys. Rev. Lett.* **124**, 105303 (2020).
- [44] T. Zhang, R. Takahashi, C. Fang, and S. Murakami, Twofold quadruple Weyl nodes in chiral cubic crystals, *Phys. Rev. B* **102**, 125148 (2020).
- [45] Q.-B. Liu, Z. Wang, and H.-H. Fu, Charge-four Weyl phonons, *Phys. Rev. B* **103**, L161303 (2021).
- [46] P.-F. Liu, J. Li, X.-H. Tu, H. Li, J. Zhang, P. Zhang, Q. Gao, and B.-T. Wang, First-principles prediction of ideal type-II Weyl phonons in wurtzite ZnSe, *Phys. Rev. B* **103**, 094306 (2021).
- [47] G. Liu, Z. Chen, P. Wu, and H. Xu, Triple hourglass Weyl phonons, *Phys. Rev. B* **106**, 214308 (2022).
- [48] X. Wang, F. Zhou, Z. Zhang, Z.-M. Yu, and Y. Yao, Hourglass charge-three Weyl phonons, *Phys. Rev. B* **106**, 214309 (2022).
- [49] X. Wang, F. Zhou, Z. Zhang, W. Wu, Z.-M. Yu, and S. A. Yang, Single pair of multi-Weyl points in nonmagnetic crystals, *Phys. Rev. B* **106**, 195129 (2022).
- [50] D. Fan, X. Wan, and F. Tang, Catalog of maximally charged Weyl points hosting nearly emanating nodal lines in phonon spectra, *Phys. Rev. B* **108**, 104110 (2023).
- [51] C. Wang, L. Jin, L. Tian, W.-W. Yu, X. Zhang, G. Liu, and Y. Liu, Multiply charged topological phonons in $K_2Pb_2O_3$, *Phys. Rev. B* **109**, 235415 (2024).
- [52] J. Liu, X. Ma, L. Sun, Z. Zhang, Y. Ni, S. Meng, and M. Zhao, Ideal type-I Weyl phonons in BA_2O_4 with fewest Weyl points, *Phys. Rev. B* **109**, 045203 (2024).
- [53] G. F. Lange, J. D. Pottecher, C. Robey, B. Monserrat, and B. Peng, Negative refraction of Weyl phonons at twin quartz interfaces, *ACS Mater. Lett.* **6**, 847 (2024).
- [54] B. Q. Lv, T. Qian, and H. Ding, Experimental perspective on three-dimensional topological semimetals, *Rev. Mod. Phys.* **93**, 025002 (2021).
- [55] B. Lv, N. Xu, H. Weng, J. Ma, P. Richard, X. Huang, L. Zhao, G. Chen, C. Matt, F. Bisti, *et al.*, Observation of Weyl nodes in TaAs, *Nat. Phys.* **11**, 724 (2015).
- [56] B. Q. Lv, H. M. Weng, B. B. Fu, X. P. Wang, H. Miao, J. Ma, P. Richard, X. C. Huang, L. X. Zhao, G. F. Chen, Z. Fang, X. Dai, T. Qian, and H. Ding, Experimental Discovery of Weyl Semimetal TaAs, *Phys. Rev. X* **5**, 031013 (2015).
- [57] S.-Y. Xu, I. Belopolski, N. Alidoust, M. Neupane, G. Bian, C. Zhang, R. Sankar, G. Chang, Z. Yuan, C.-C. Lee, *et al.*, Discovery of a Weyl fermion semimetal and topological Fermi arcs, *Science* **349**, 613 (2015).
- [58] L. Yang, Z. Liu, Y. Sun, H. Peng, H. Yang, T. Zhang, B. Zhou, Y. Zhang, Y. Guo, M. Rahn, *et al.*, Weyl semimetal phase in the non-centrosymmetric compound TaAs, *Nat. Phys.* **11**, 728 (2015).
- [59] K. Deng, G. Wan, P. Deng, K. Zhang, S. Ding, E. Wang, M. Yan, H. Huang, H. Zhang, Z. Xu, *et al.*, Experimental observation of topological Fermi arcs in type-II Weyl semimetal MoTe₂, *Nat. Phys.* **12**, 1105 (2016).
- [60] Y. Wu, D. Mou, N. H. Jo, K. Sun, L. Huang, S. L. Bud'ko, P. C. Canfield, and A. Kaminski, Observation of Fermi arcs in the type-II Weyl semimetal candidate WTe₂, *Phys. Rev. B* **94**, 121113 (2016).
- [61] H. Miao, T. T. Zhang, L. Wang, D. Meyers, A. H. Said, Y. L. Wang, Y. G. Shi, H. M. Weng, Z. Fang, and M. P. M. Dean, Observation of Double Weyl Phonons in Parity-Breaking FeSi, *Phys. Rev. Lett.* **121**, 035302 (2018).
- [62] J. Li, J. Li, J. Tang, Z. Tao, S. Xue, J. Liu, H. Peng, X.-Q. Chen, J. Guo, and X. Zhu, Direct Observation of Topological Phonons in Graphene, *Phys. Rev. Lett.* **131**, 116602 (2023).
- [63] T. T. Zhang, H. Miao, Q. Wang, J. Q. Lin, Y. Cao, G. Fabbris, A. H. Said, X. Liu, H. C. Lei, Z. Fang, H. M. Weng, and M. P. M. Dean, Phononic Helical Nodal Lines with \mathcal{PT} Protection in MoB₂, *Phys. Rev. Lett.* **123**, 245302 (2019).
- [64] Z. Jin, B. Hu, Y. Liu, Y. Li, T. Zhang, K. Iida, K. Kamazawa, A. I. Kolesnikov, M. B. Stone, X. Zhang, H. Chen, Y. Wang, I. A. Zaliznyak, J. M. Tranquada, C. Fang, and Y. Li, Chern numbers of topological phonon band crossing determined with inelastic neutron scattering, *Phys. Rev. B* **106**, 224304 (2022).
- [65] A. A. Zyuzin and A. A. Burkov, Topological response in Weyl semimetals and the chiral anomaly, *Phys. Rev. B* **86**, 115133 (2012).
- [66] D. T. Son and B. Z. Spivak, Chiral anomaly and classical negative magnetoresistance of Weyl metals, *Phys. Rev. B* **88**, 104412 (2013).
- [67] M. M. Vazifeh and M. Franz, Electromagnetic Response of Weyl Semimetals, *Phys. Rev. Lett.* **111**, 027201 (2013).
- [68] S. A. Parameswaran, T. Grover, D. A. Abanin, D. A. Pesin, and A. Vishwanath, Probing the Chiral Anomaly with Nonlocal Transport in Three-Dimensional Topological Semimetals, *Phys. Rev. X* **4**, 031035 (2014).
- [69] C.-X. Liu, P. Ye, and X.-L. Qi, Chiral gauge field and axial anomaly in a Weyl semimetal, *Phys. Rev. B* **87**, 235306 (2013).
- [70] X. Huang, L. Zhao, Y. Long, P. Wang, D. Chen, Z. Yang, H. Liang, M. Xue, H. Weng, Z. Fang, X. Dai, and G. Chen, Observation of the Chiral-Anomaly-Induced Negative Magnetoresistance in 3D Weyl Semimetal TaAs, *Phys. Rev. X* **5**, 031023 (2015).
- [71] H.-J. Kim, K.-S. Kim, J.-F. Wang, M. Sasaki, N. Satoh, A. Ohnishi, M. Kitaura, M. Yang, and L. Li, Dirac versus Weyl Fermions in Topological Insulators: Adler-Bell-Jackiw Anomaly in Transport Phenomena, *Phys. Rev. Lett.* **111**, 246603 (2013).
- [72] Y. X. Zhao and S. A. Yang, Index Theorem on Chiral Landau Bands for Topological Fermions, *Phys. Rev. Lett.* **126**, 046401 (2021).
- [73] J. Xiong, S. K. Kushwaha, T. Liang, J. W. Krizan, M. Hirschberger, W. Wang, R. J. Cava, and N. P. Ong, Evidence for the chiral anomaly in the Dirac semimetal Na₃Bi, *Science* **350**, 413 (2015).
- [74] V. Könye, A. Bouhon, I. C. Fulga, R.-J. Slager, J. van den

- Brink, and J. I. Facio, Chirality flip of Weyl nodes and its manifestation in strained MoTe_2 , *Phys. Rev. Res.* **3**, L042017 (2021).
- [75] E. Thareja, G. Pantano, I. Vekhter, and J. Gayles, Tuning Quantum States at Chirality-Reversed Planar Interface in Weyl Semimetals using an Interstitial Layer, arXiv:2501.05594 (2025).
- [76] N. Yoshikawa, K. Ogawa, Y. Hirai, K. Fujiwara, J. Ikeda, A. Tsukazaki, and R. Shimano, Non-volatile chirality switching by all-optical magnetization reversal in ferromagnetic Weyl semimetal $\text{Co}_3\text{Sn}_2\text{S}_2$, *Commun. Phys.* **5**, 328 (2022).
- [77] S. Liu, Y. Kim, L. Z. Tan, and A. M. Rappe, Strain-induced ferroelectric topological insulator, *Nano Lett.* **16**, 1663 (2016).
- [78] A. Narayan, Class of Rashba ferroelectrics in hexagonal semiconductors, *Phys. Rev. B* **92**, 220101 (2015).
- [79] D. Di Sante, P. Barone, A. Stroppa, K. F. Garrity, D. Vanderbilt, and S. Picozzi, Intertwined Rashba, Dirac, and Weyl Fermions in Hexagonal Hyperferroelectrics, *Phys. Rev. Lett.* **117**, 076401 (2016).
- [80] B. Monserrat, J. W. Bennett, K. M. Rabe, and D. Vanderbilt, Antiferroelectric Topological Insulators in Orthorhombic AMgBi Compounds ($A = \text{Li}, \text{Na}, \text{K}$), *Phys. Rev. Lett.* **119**, 036802 (2017).
- [81] N. Mao, R. Li, X. Zou, Y. Dai, B. Huang, and C. Niu, Ferroelectric higher-order topological insulator in two dimensions, *Phys. Rev. B* **107**, 045125 (2023).
- [82] N.-J. Yang, J.-M. Zhang, X.-P. Li, Z. Zhang, Z.-M. Yu, Z. Huang, and Y. Yao, Sliding Ferroelectrics Induced Hybrid-Order Topological Phase Transitions, *Phys. Rev. Lett.* **134**, 256602 (2025).
- [83] X.-W. Zhao, S.-N. Dong, G.-Y. Gao, Z.-X. Xu, M. Xu, J.-M. Yan, W.-Y. Zhao, Y.-K. Liu, S.-Y. Yan, J.-X. Zhang, *et al.*, Reversible and nonvolatile manipulation of the electronic transport properties of topological insulators by ferroelectric polarization switching, *npj Quantum Mater.* **3**, 52 (2018).
- [84] P. Sharma, F.-X. Xiang, D.-F. Shao, D. Zhang, E. Y. Tsymbal, A. R. Hamilton, and J. Seidel, A room-temperature ferroelectric semimetal, *Sci. Adv.* **5**, eaax5080 (2019).
- [85] R. Li, Y. Xu, J. He, S. Ullah, J. Li, J.-M. Liu, D. Li, C. Franchini, H. Weng, and X.-Q. Chen, Weyl ferroelectric semimetal, arXiv:1610.07142 (2016).
- [86] C. Bradley and A. Cracknell, *The mathematical theory of symmetry in solids: representation theory for point groups and space groups* (Oxford University Press, 2009).
- [87] See the Supplemental Material for a more detailed table of candidate space groups, computational methods, the whole phonon spectrum of K_2ZnBr_4 and other materials in the A_2BX_4 family ($A = \text{Rb}, \text{K}$; $B = \text{Zn}, \text{Co}$; $X = \text{Cl}, \text{Br}, \text{I}$), the Wilson loop spectrum, and the $k \cdot p$ model of Weyl points. Also included are chirality switchable Weyl phonon materials with high Chern numbers ($C = 2$ and 3), namely $\text{Y}(\text{OH})_3$ and LiIO_3 , as well as the symmetry requirements for the nonlinear phonon Hall effect in K_2ZnBr_4 materials, which includes Refs. [90, 92–98].
- [88] F. Shimizu, T. Yamaguchi, H. Suzuki, M. Takashige, and S. Sawada, New Ferroelectric K_2ZnBr_4 , *J. Phys. Soc. Jpn.* **59**, 1936 (1990).
- [89] C. Fang, L. Lu, J. Liu, and L. Fu, Topological semimetals with helicoid surface states, *Nat. Phys.* **12**, 936 (2016).
- [90] W. Luo, J. Ji, P. Chen, Y. Xu, L. Zhang, H. Xiang, and L. Bellaïche, Nonlinear phonon Hall effects in ferroelectrics: Existence and nonvolatile electrical control, *Phys. Rev. B* **107**, L241107 (2023).
- [91] H. Chen, W. Wu, K. Sun, S. A. Yang, and L. Zhang, Electrically controllable chiral phonons in ferroelectric materials, *Appl. Phys. Lett.* **124** (2024).
- [92] G. Kresse and J. Furthmüller, Efficient iterative schemes for ab initio total-energy calculations using a plane-wave basis set, *Phys. Rev. B* **54**, 11169 (1996).
- [93] J. P. Perdew, K. Burke, and M. Ernzerhof, Generalized Gradient Approximation Made Simple, *Phys. Rev. Lett.* **77**, 3865 (1996).
- [94] G. Henkelman, B. P. Uberuaga, and H. Jónsson, A climbing image nudged elastic band method for finding saddle points and minimum energy paths, *J. Chem. Phys.* **113**, 9901 (2000).
- [95] A. Togo and I. Tanaka, First principles phonon calculations in materials science, *Scr. Mater.* **108**, 1 (2015).
- [96] Q. Wu, S. Zhang, H.-F. Song, M. Troyer, and A. A. Soluyanov, WannierTools: An open-source software package for novel topological materials, *Comput. Phys. Commun.* **224**, 405 (2018).
- [97] G. Beall, W. Milligan, and H. A. Wolcott, Structural trends in the lanthanide trihydroxides, *J. Inorg. Nucl. Chem.* **39**, 65 (1977).
- [98] E. Coquet, J. Crettez, J. Pannetier, J. Bouillot, and J. Damien, Effect of temperature on interatomic distances in pyroelectric $\alpha\text{-LiIO}_3$, *Acta Crystallogr. B* **39**, 408 (1983).